MIT Libraries | DSpace@MIT

MIT Open Access Articles

Accumulation of collagen molecular unfolding is the mechanism of cyclic fatigue damage and failure in collagenous tissues

The MIT Faculty has made this article openly available. ***Please share*** how this access benefits you. Your story matters.

Citation: Zitnay, Jared L, Jung, Gang Seob, Lin, Allen H, Qin, Zhao, Li, Yang et al. 2020. "Accumulation of collagen molecular unfolding is the mechanism of cyclic fatigue damage and failure in collagenous tissues." Science Advances, 6 (35).

As Published: 10.1126/SCIADV.ABA2795

Publisher: American Association for the Advancement of Science (AAAS)

Persistent URL: https://hdl.handle.net/1721.1/132713

Version: Final published version: final published article, as it appeared in a journal, conference proceedings, or other formally published context

Terms of use: Creative Commons Attribution NonCommercial License 4.0

Massachusetts Institute of Technology

PHYSIOLOGY

Accumulation of collagen molecular unfolding is the mechanism of cyclic fatigue damage and failure in collagenous tissues

Jared L. Zitnay[1,2], Gang Seob Jung[3]*, Allen H. Lin[1,2], Zhao Qin[3†], Yang Li[1], S. Michael Yu[1,4], Markus J. Buehler[3], Jeffrey A. Weiss[1,2,5‡]

Copyright © 2020 The Authors, some rights reserved; exclusive licensee American Association for the Advancement of Science. No claim to original U.S. Government Works. Distributed under a Creative Commons Attribution NonCommercial License 4.0 (CC BY-NC).

Overuse injuries to dense collagenous tissues are common, but their etiology is poorly understood. The predominant hypothesis that micro-damage accumulation exceeds the rate of biological repair is missing a mechanistic explanation. Here, we used collagen hybridizing peptides to measure collagen molecular damage during tendon cyclic fatigue loading and computational simulations to identify potential explanations for our findings. Our results revealed that triple-helical collagen denaturation accumulates with increasing cycles of fatigue loading, and damage is correlated with creep strain independent of the cyclic strain rate. Finite-element simulations demonstrated that biphasic fluid flow is a possible fascicle-level mechanism to explain the rate dependence of the number of cycles and time to failure. Molecular dynamics simulations demonstrated that triple-helical unfolding is rate dependent, revealing rate-dependent mechanisms at multiple length scales in the tissue. The accumulation of collagen molecular denaturation during cyclic loading provides a long-sought "micro-damage" mechanism for the development of overuse injuries.

INTRODUCTION

Dense collagenous tissues such as tendon, ligament, cartilage, intervertebral disc, bone, and skin are incredible natural structures capable of sustaining millions of loading cycles over a lifetime. Although these tissues typically perform their physiological functions for decades without injury or permanent dysfunction, overuse-related injuries such as tendinosis, rotator cuff disease, bursitis, osteoarthritis, and bone fragility fractures are common clinical pathologies that can be difficult to treat. The predominant hypothesis for the development of overuse injuries is that repeated subfailure loading cycles cause the accumulation of "micro-damage" in one or more structural components in the tissue (*1*). When the rate of micro-damage accumulation exceeds the rate of biological repair, injury or failure occurs under normal loading conditions. While it is expected that this micro-damage accumulates at one or more levels of the tissue's structural hierarchy, relatively little is known about the mechanisms of micro-damage that potentiate overuse pathologies. Knowledge of these mechanisms would present a very important advancement for understanding the etiology of these common injuries and ultimately improving options for their treatment and prevention.

In the context of overuse injuries to collagenous tissues, tendons are often studied as they have a relatively simple structure composed almost entirely of collagen fibrils arranged in parallel, and because a number of clinically relevant overuse pathologies involve tendons. Tendons will ultimately fail when subjected to cyclic loading at subfailure levels of stress (cyclic fatigue loading) in vitro, demonstrating a finite fatigue life (*2*, *3*). After tendons are subjected to cyclic fatigue loading, they exhibit disorganization and kinking of the collagen fibers and fibrils (*4*–*6*), altered fiber crimp (*7*), collagen denaturation (*6*), and reduced tensile strength and tissue modulus (*4*, *8*). Thus, it is clear that damage to collagen, the primary structural component of tendon, is involved in the micro-damage process. Yet, the underlying cause of damage accumulation during cyclic fatigue loading in tendons and the possible role of collagen molecular damage in this process are unknown.

Previously, we used fluorescently labeled collagen hybridizing peptide (F-CHP) to demonstrate that the collagen molecules in tendon fascicles become permanently unfolded, or denatured, when subjected to a single quasistatic tensile overload event (*9*). CHP is a small synthetic peptide with glycine-proline-hydroxyproline repeats that has a strong propensity to fold into the triple-helical super-secondary protein structure of native collagens and can hybridize with unfolded collagen α chains (*10*). CHP binding revealed molecular-level collagen damage at subfailure strains, and damage increased with higher strain levels. The accumulation of collagen damage with increasing strain followed the same pattern as the strain-dependent increase of trypsin solubility in monotonically loaded tendons, demonstrating that the collagen denaturation previously detected using trypsin degradation (*11*–*13*) was indeed mechanically unfolded collagen molecules. Molecular dynamics (MD) simulations revealed that the likely mechanism of mechanical unfolding of the triple helix is due to shear load transfer and individual α-chain pullout (*9*).

Here, we investigated the role of molecular-level collagen damage during cyclic fatigue loading in tendon fascicles and identified molecular mechanisms for the initiation and accumulation of this damage (Fig. 1). Given the critical role of mechanical unfolding of collagen triple helix during monotonic tension loading and our understanding of the collagen triple helix as the base structural unit

[1]Department of Biomedical Engineering, University of Utah, Salt Lake City, UT 84112, USA. [2]Scientific Computing and Imaging Institute, University of Utah, Salt Lake City, UT 84112, USA. [3]Laboratory for Atomistic and Molecular Mechanics, Department of Civil and Environmental Engineering, Massachusetts Institute of Technology, Cambridge, MA 02139, USA. [4]Department of Pharmaceutics and Pharmaceutical Chemistry, University of Utah, Salt Lake City, UT 84132, USA. [5]Department of Orthopaedics and School of Computing, University of Utah, Salt Lake City, UT 84112, USA.
*Present address: Computational Sciences and Engineering Division, Oak Ridge National Laboratory, Oak Ridge, TN 37831, USA.
†Present address: Civil and Environmental Engineering, Syracuse University, Syracuse, NY 13244, USA.
‡Corresponding author. Email: jeff.weiss@utah.edu

Downloaded from https://www.science.org on October 04, 2021

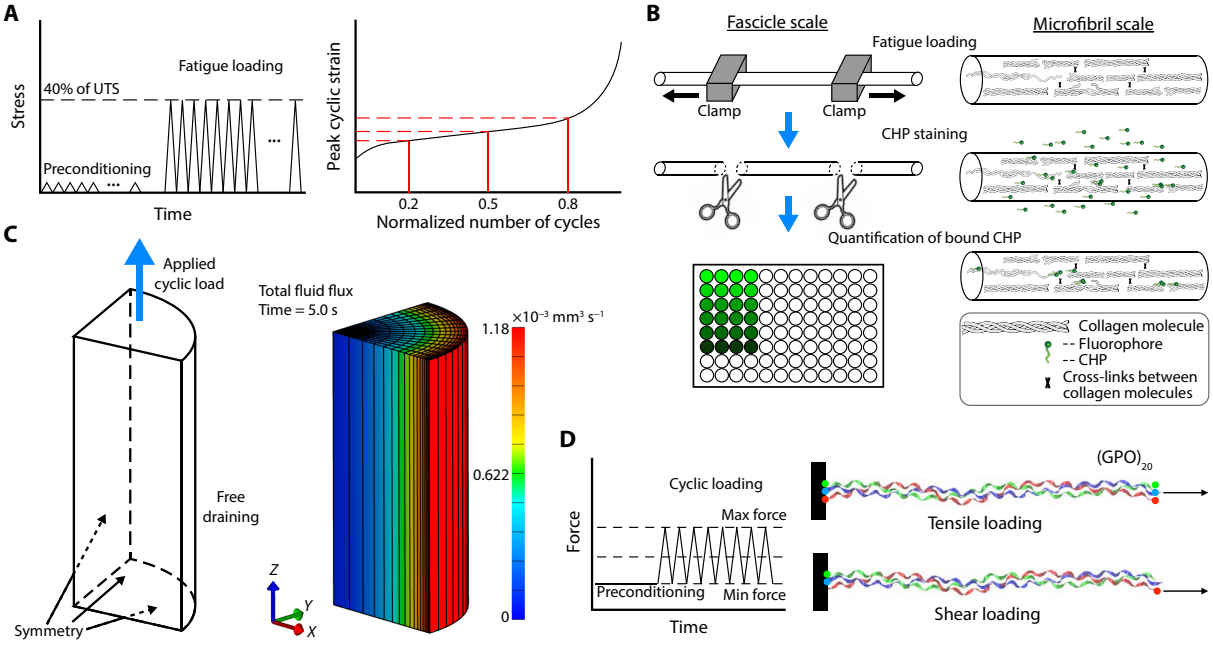

Fig. 1. Study overview. (**A**) Rat tail tendon fascicles were loaded in creep-fatigue to 40% of the ultimate tensile strength (UTS) until tissue failure. Incremental levels of fatigue were defined as the peak cyclic (creep) strain at 20, 50, and 80% of cycles to failure. (**B**) To label and quantify denatured collagen, we stained mechanically loaded fascicles with fluorescent CHP, which hybridizes to unfolded collagen α chains. The amount of denatured collagen was quantified on microplate via the fluorescence of bound F-CHP. Computational simulations were used to investigate the potential mechanisms of fascicle- and molecular-level fatigue behavior. (**C**) Biphasic finite-element simulations were used to study the potential role of fluid flow on strain rate–dependent fatigue behavior at the fascicle level. (**D**) MD simulations of collagen model peptides were used to identify molecular mechanisms of fatigue damage accumulation and strain rate dependence. GPO, glycine-proline-hydroxyproline.

of the collagen architecture, the overarching hypothesis of this research was that molecular-level collagen damage is fundamental to the initiation and progression of damage, and ultimately failure, during cyclic fatigue loading of tendon. We further hypothesized that collagen molecular damage is the mechanism responsible for tissue creep, the increased length observed when a tendon is held under static loading or cycled to the same load. We used F-CHP to detect and quantify triple-helical collagen damage in rat tail tendon (RTT) fascicles subjected to incremental levels of creep-fatigue. The molecular mechanisms of fatigue damage and mechanisms of loading rate dependence were investigated using continuum-level finite-element simulations and atomic-scale steered MD (SMD) simulations. This study demonstrates that collagen molecular damage accumulates over the course of cyclic fatigue loading, identifying the mechanism for micro-damage accumulation and ultimately failure of the tissue, and demonstrates that both fascicle-level fluid flow and atomic-level interactions during triple-helix unfolding contribute to the rate dependence of fatigue damage accumulation and fatigue failure.

RESULTS

Collagen molecular damage accumulates during cyclic fatigue loading

To determine the role of molecular-level collagen mechanical damage during tendon fatigue, we loaded RTT fascicles in cyclic creep until failure or reaching one of three predetermined subfailure strains, representing increasing levels of fatigue. When samples were loaded until failure, they exhibited the expected triphasic creep pattern (*4*, *14*), in which peak cyclic strain (strain measured at the peak of the loading cycle) rapidly increased over the first loading cycles, with slower and nearly linear increase over the majority of loading cycles, and again increasing rapidly in the loading cycles just before failure (Fig. 2A). Samples were loaded at 4% s^{-1} strain rate, which resulted in 0.97 ± 0.17 Hz (mean ± SD) cyclic frequency at 50% of cycles to failure, achieving a loading frequency similar to human walking. Throughout tendon fatigue, the secant modulus also exhibited a triphasic pattern: decreasing rapidly during the primary phase, followed by a slower and nearly linear decrease during the secondary phase, and again rapidly decreasing immediately before failure (fig. S1).

To measure the amount of collagen damage caused by mechanical fatigue loading, we stained samples with F-CHP to specifically label unfolded collagens. The percent of collagen denaturation was measured using a microplate fluorescence assay calibrated to the trypsin-hydroxyproline assay, as previously reported (*15*). The amount of denatured collagen due to fatigue loading increased with the number of loading cycles relative to failure ($P < 0.001$; Fig. 2B), with noticeable molecular damage at the lowest level of loading (20% of cycles to failure). CHP quantification demonstrated that permanent molecular damage begins early during the secondary phase of creep and accumulates through the creep-fatigue process, suggesting that mechanical unfolding of the collagen triple helix is a critical feature of tendon fatigue damage.

Collagen molecular damage evolves with increasing creep strain, independent of strain rate

Because tendons experience a wide range of strain rates in vivo, we performed additional fatigue loading experiments at 0.4 and 40% s^{-1} to understand the evolution of molecular damage across the

Downloaded from https://www.science.org on October 04, 2021

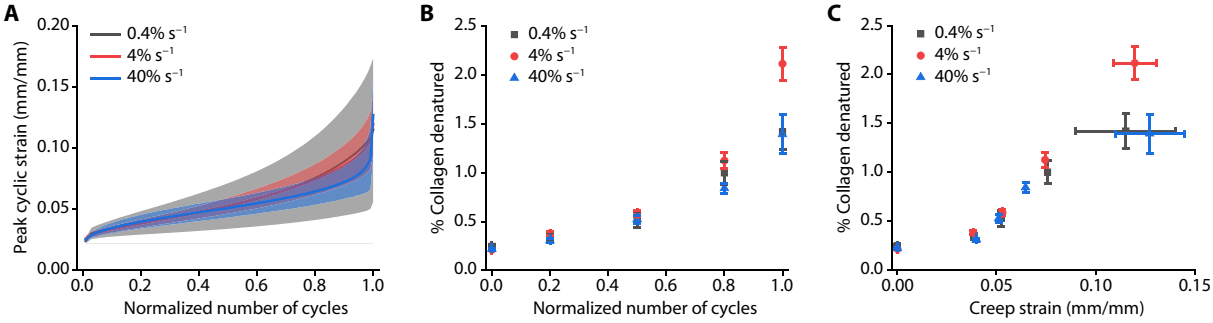

Fig. 2. Fascicle-level tendon creep and molecular-level mechanical damage to collagen during cyclic creep loading. (**A**) All samples exhibited creep behavior, with the sample strain increasing with additional cycles to the same stress level. A triphasic creep pattern was observed at all strain rates; high rates of creep were observed in the initial and final loading cycles, with steady-state creep rate for the majority of the loading duration. While the mean peak cyclic strain was not significantly different between strain rates ($P = 0.756$; $n = 10$ per strain rate), there was less variation in the peak cyclic strain at higher strain rates, indicated by the smaller shaded region of SD. (**B**) Denatured collagen accumulated in the samples throughout the fatigue loading process ($P < 0.001$; $n \geq 5$ per group), with a noticeable increase as early as the strain corresponding to only 20% of cycles to failure. However, the amount of denatured collagen as a function of the normalized number of loading cycles was similar between strain rates ($P = 0.179$). (**C**) Plotting the amount of collagen that was mechanically denatured against the peak cyclic strain of the sample reveals the strong correlation of damage with applied strain, without a significant effect of the strain rate of the cyclic loading. These data reveal an apparent damage threshold between 0 and 20% of cycles to failure and between 0 and ~3.8% strain. Mean ± SD in (A) and mean ± SE in (B) and (C).

range from repeated quasistatic to physiologically relevant loading rates. The cyclic frequency measured at 50% of cycles to failure was 0.11 ± 0.04 Hz and 8.55 ± 0.86 Hz (mean ± SD) at 0.4 and 40% s^{-1}, respectively. For comparison, the typical range of running stride frequency is 1 to 4 Hz in humans and 4 to 8 Hz in small rodents (*16*, *17*). Samples cycled until failure again exhibited the triphasic creep pattern. When the loading cycle was normalized to the number of cycles at failure, neither the peak cyclic strain (Fig. 2A) nor the secant modulus (fig. S1) was significantly different between strain rates ($P = 0.756$ and $P = 0.884$, respectively). We observed less variation in the peak cyclic strain at increased loading rates (Fig. 2A). The amount of denatured collagen as a function of normalized number of cycles also did not exhibit a strain rate effect ($P = 0.210$) nor an interaction between strain rate and level of fatigue ($P = 0.468$), indicating that similar amounts of collagen molecular damage result from loading to the same relative level of fatigue (Fig. 2B).

Considering the strain rate independence of both peak cyclic strain and collagen damage, it is informative to consider the amount of collagen damage as a function of the creep strain. There was a strong correlation between collagen damage and creep strain, independent of strain rate, suggesting a mechanistic relationship between these two measures of fatigue (Fig. 2C). We observed that the amount of denatured collagen present after fatigue loading, both at intermediate fatigue levels and failure, was similar to the amounts measured previously using trypsin solubility and CHP detection of denatured collagen in monotonically strained samples (*9*, *12*, *15*). This consistent relationship between the amount of collagen molecular damage and applied mechanical strain—regardless of strain rate or strain history—indicates that molecular damage is a strain-dependent process.

The time scale of fatigue damage is rate dependent

Although the evolution of both fascicle- and molecular-level measures of fatigue (i.e., creep strain and collagen unfolding) were independent of strain rate, the time scale of damage accumulation and the cyclic lifetime were strongly influenced by the loading rate. There was a significant effect of strain rate on both the number of cycles to failure (Fig. 3A) and the time to failure ($P < 0.001$ and $P = 0.003$, respectively) (Fig. 3B and fig. S2); although higher loading rates required more cycles to cause catastrophic tissue failure, the failure occurred faster. Thus, while the amount and rate of collagen damage accumulation as a function of normalized cycles were independent of loading rate, the damage accumulated faster at higher loading rates. Contrarily, there was more than an order of magnitude increase in the number of cycles required to reach failure at the fastest loading rate, indicating that RTT has greater resistance to fatigue loading cycles during faster loading. Increased strength at faster loading rates could explain the increased fatigue resistance and account for why the same number of loading cycles to the same peak stress was less damaging at 40% s^{-1} than at 0.4% s^{-1}. To assess this possibility, we tested additional RTT in monotonic tension to failure at 0.4, 4, and 40% s^{-1}, which demonstrated that there was a significant effect of loading rate on effective tissue strength ($P < 0.001$; Fig. 3C). Our result is consistent with the strain rate–dependent ultimate tensile strength (UTS) previously reported for ligament and tendon (*18*) and correlates with the strain rate–dependent increase in the number of loading cycles to failure that we observed.

The biphasic nature of connective tissues provides a demonstrated mechanism in which fluid content and fluid flow relative to the solid tissue structure can both influence quasistatic tissue mechanics and impart rate-dependent behavior (*19*, *20*). To investigate whether a fluid flow–based mechanism could explain the observed rate-dependent fatigue resistance, we performed finite-element simulations using an anisotropic, high Poisson's ratio permeable elastic solid with a mobile fluid phase (Fig. 1C). The Poisson's ratio of tendons and ligaments has been demonstrated to be much greater than the theoretical incompressibility limit (*21*), implying that the magnitude of lateral compressive strains during uniaxial extension can exceed the magnitude of the applied tensile strains and force fluid out of the tissue. We investigated the model behavior under 0.1-, 1-, and 10-Hz cyclic frequency, with minimum and maximum stress levels corresponding to experiments (2.62 to 18.49 MPa). Unlike native tendon, the simulated elastic material ultimately achieved equilibrium under cyclic loading rather than experiencing failure, with all models displaying similar time to reach equilibrium. As a comparison, we considered model equilibrium to be roughly equivalent to the start of the secondary phase of fatigue creep. The number of cycles required

Downloaded from https://www.science.org on October 04, 2021

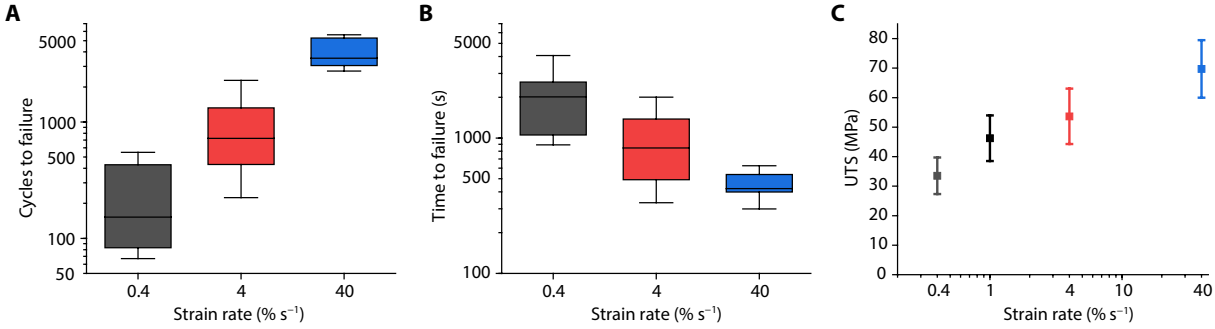

Fig. 3. Strain rate dependence of fatigue failure and effective material strength. Strain rate had a significant effect on both (**A**) the number of cycles to failure ($P < 0.001$; $n = 10$ per strain rate) and (**B**) time to fatigue failure ($P = 0.003$; $n = 10$ per strain rate). While samples required more loading cycles to failure at increased strain rates, they failed in less time. This strain rate dependence of both cycles and time to failure demonstrates that tendon creep-fatigue failure is not a pure creep process, which would be dependent only on the time under strain. (**C**) The monotonic UTS also exhibited significant strain rate dependence ($P < 0.001$; $n = 18$ for 0.4% s^{-1}, $n = 12$ for 1% s^{-1}, and $n = 15$ for 4 and 40% s^{-1}). The strain rate–dependent UTS may contribute to samples enduring more loading cycles at higher strain rate under the same stress magnitude, as they are being loaded to a lower stress relative to the effective tissue strength. Median ± interquartile range (IQR) with bars representing the range within 1.5 IQR in (A) and (B) and mean ± SD in (C).

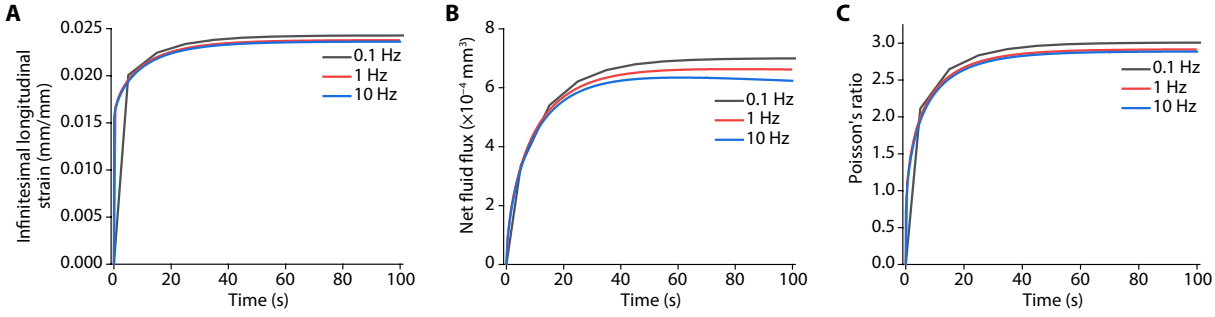

Fig. 4. Biphasic rate dependence of tendon mechanics under simulated cyclic loading. (**A**) Finite-element simulations predicted tendon creep during cyclic loading with strain at the loading peak reaching an equilibrium around 50 s, which was similar to the transition time from the primary to the secondary phase of fatigue in experiments. The similar equilibrium time between cyclic frequencies revealed that more cycles were required to reach equilibrium at higher frequency. (**B**) Fluid exudation was predicted to increase with time during cyclic loading, and (**C**) the lateral contraction (Poisson's ratio) at the loading peak correspondingly increased. Similar to strain, more cycles were required to reach equilibrium at higher frequencies. Thus, more fluid exuded with each loading cycle at lower frequency, decreasing the material cross-sectional area and increasing the amount of stress on the solid phase. All graphs plot the values at the peak of each loading cycle.

to reach equilibrium increased with cyclic frequency only when the solid material was used in a biphasic formulation (Fig. 4 and figs. S3 and S4), demonstrating that fluid flow is a realistic mechanism for rate-dependent cyclic behavior. There was greater net fluid exudation per loading cycle at slower loading rates (Fig. 4B), which provides insight into the biphasic mechanism for rate-dependent fatigue damage: Increased fluid exudation causes a corresponding reduction in cross-sectional area (CSA) (Fig. 4C), thus increasing the relative stress borne by the remaining solid phase. Understanding the complex interplay between loading rate, number of loading cycles, and the time scale of damage accumulation may prove useful for the evaluation of tendon injury risk across the range of repetitive motions.

The collagen triple helix exhibits progressive unfolding and eventual catastrophic failure under cyclic loading

To understand the mechanism responsible for collagen damage accumulation during cyclic fatigue at the molecular level, we performed SMD simulations of collagen model peptides under cyclic loading. We simulated both shear- and tension-dominant loading, which correspond to shear load transfer via intermolecular cross-links and direct stretching of the triple helix, respectively (Fig. 1D). Under shear-dominant loading, the triple helix exhibited creep elongation under cyclic loading, progressive unfolding as indicated by increased solvent-accessible surface area (SASA), disruption of intermolecular hydrogen bonding, and eventual failure via catastrophic α-chain sliding (Fig. 5). Consistent with our previous SMD simulations of monotonic loading (*9*), the triple helix was mechanically stable under tension-dominant cyclic loading (fig. S5). The accumulation of molecular strain and unfolding with additional loading cycles demonstrates that triple-helical unfolding is a fundamental mechanism of permanent tissue creep due to cyclic loading. Furthermore, creep strain and triple-helical unfolding accumulated in a rate-dependent manner, with higher strain rates requiring more loading cycles to reach the same level of strain and triple-helical disruption.

The rate dependence of the triple-helical unfolding of the collagen molecule reveals a possible molecular mechanism for fascicle-level rate dependence, independent of the biphasic mechanism discussed above. Under monotonic loading, the hydrogen bond network of the triple helix and its change in the collagen peptides controls the rate dependence of structural deformation and thus the mechanical response that originates from covalent bonds (*22*). Our simulations

Downloaded from https://www.science.org on October 04, 2021

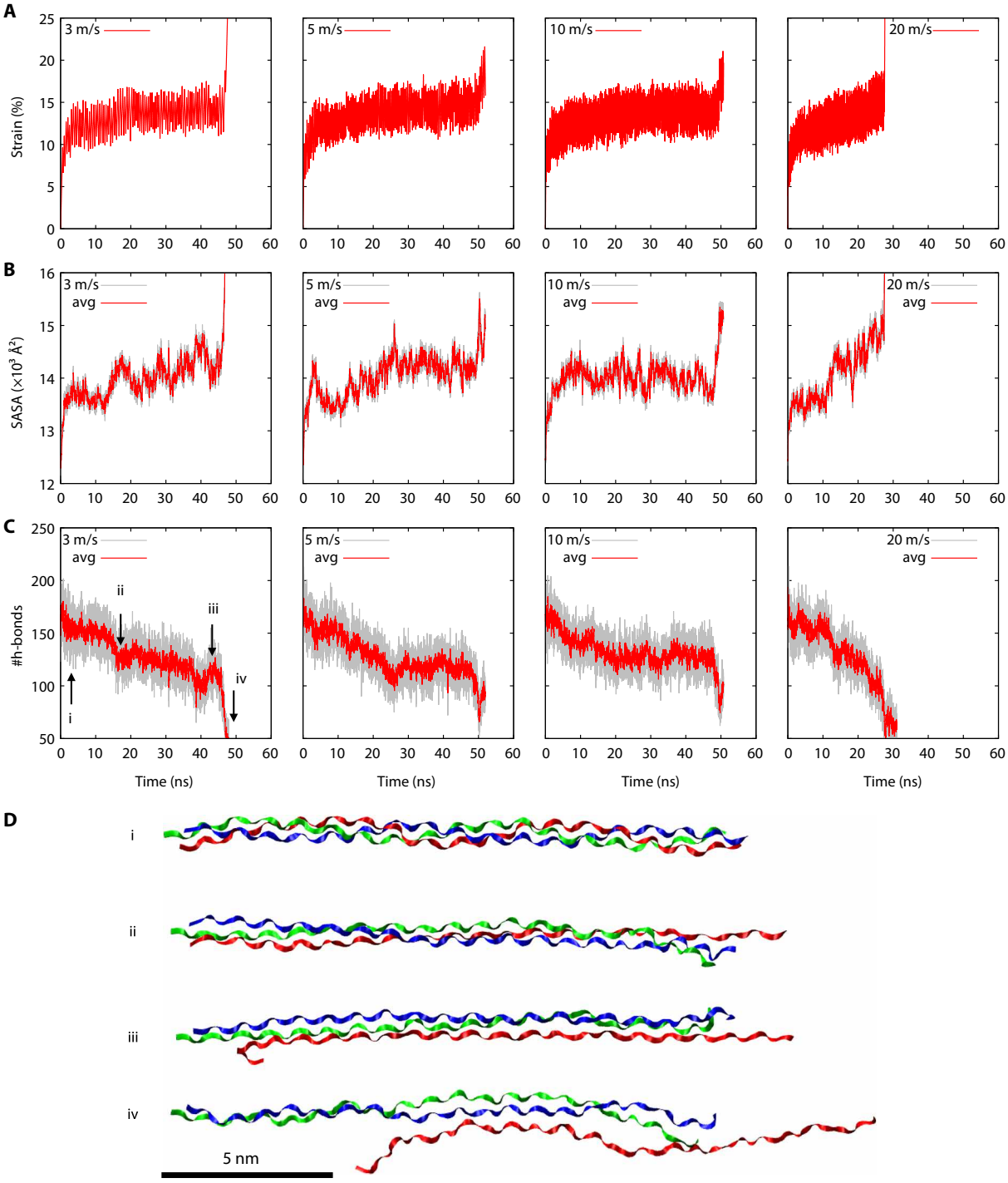

Fig. 5. Simulated fatigue failure of the triple-helix collagen peptide due to shear-dominant loading. Triple-helix peptides were subjected to repeated cycles of shear-dominant loading between constant force levels, at four different displacement rates. (**A** to **C**) Cyclic equilibrium did not exist at any of the displacement rates simulated. Although molecules did not follow the same log-linear correlation of time to failure and strain rate as experiments, the triple helix loaded at 10 m/s or slower exhibited longer times to failure than at 20 m/s. The consistent time to failure at or below a displacement rate of 10 m/s suggests that the failure of individual triple helices is a creep-dominant mechanism, while fascicle-level fatigue failure (i.e., assemblies of molecules) was not entirely explained by creep. avg, average. (**D**) Triple-helix damage progressed by unraveling and unfolding with catastrophic failure occurring via α-chain pullout. Simulation snapshots correspond to points identified for the simulation in (C).

Downloaded from https://www.science.org on October 04, 2021

suggest that the rate dependence under cyclic loading may originate from the same atomic-level mechanism, with weaker hydrogen bonds dominating the slow rate response and covalent peptide bonds dominating the fast rate response. It is likely that multiple mechanisms at different length scales are required to generate the complex rate dependence of both time and the number of loading cycles on fatigue damage observed in experiments, including but not limited to poroelasticity at the fascicle level and triple-helical unfolding at the molecular level. The MD simulations were able to model failure behavior, demonstrating that continued cycling causes catastrophic disruption of the triple-helix structure that would destabilize molecular organization within fibrils and reduce the tissue's load-bearing capacity. While these simulations demonstrated creep-fatigue behavior in individual triple-helix molecules, we previously demonstrated that the mechanisms identified in these simulations are conserved in simulated arrays of full-length collagen molecules containing at least two known intermolecular cross-links (*9*).

DISCUSSION

The micro-damage hypothesis presents a widely accepted explanation for the development of repetitive loading-related pathologies in collagenous tissues: Small amounts of structural damage are created because of repeated subfailure loading and can accumulate when damage creation outpaces repair (*1*). However, the actual sources and mechanisms of micro-damage creation and accumulation have remained elusive. We have demonstrated that cyclic loading of tendon fascicles results in the accumulation of denatured collagen due to mechanical unfolding even at relatively low numbers of cycles. Thus, mechanical unfolding of the collagen triple helix is a critical feature of damage accumulation in tendons during cyclic fatigue loading. From MD simulations, it is clear that progressive unfolding of the triple-helix structure exhibits similar creep behavior and loading rate dependence observed at the level of the tendon fascicle. Thus, mechanical unfolding of the collagen triple helix may be the foundational mechanism responsible for the generation of fascicle-level creep strain under cyclic loading. Together, these results provide a convincing explanation for the micro-damage hypothesis in dense collagenous tissues: Molecular-level collagen damage is generated because of tissue-level mechanical loading, and the ability to repair damage to the most basic level of the collagen structure determines whether the applied loading leads to tissue failure.

Our results demonstrated key rate dependencies for fatigue resistance and fatigue lifetime. We used computational simulations to explore mechanisms at the tissue and molecular levels that could contribute to this rate dependence. In continuum finite-element simulations, we examined the role of biphasic fluid flow and demonstrated that greater net flux per loading cycle at slower cyclic frequencies leads to more tissue creep. These results also suggest a possible fluid-based mechanism modulating molecular-level damage, as increased fluid exudation and corresponding CSA reduction per loading cycle would increase the relative stress on the collagen matrix. In the context of a biphasic mixture material undergoing fatigue damage, this loss of fluid load support could contribute to a lower fatigue resistance of the solid phase at slower loading rates. Atomistic-scale MD simulations elucidated rate dependence, deformation, and damage mechanisms at the level of the collagen triple helix. These simulations revealed molecular-level creep and fatigue damage behavior due to triple helix unfolding, demonstrating that the triple-helix structure is capable of fatigue rupture. The SMD results also predicted more molecular-level creep and helix unfolding per loading cycle at slower loading rates, revealing a potential molecular mechanism to explain the loading rate dependence of fatigue resistance. Both computational models exhibited similar time scales of fatigue behavior across loading rates, but experiments clearly showed an inverse correlation between fatigue lifetime and strain rate. This discrepancy suggests a potential coupling between tissue and molecular-level mechanisms and that the distribution of damage among arrays of collagen molecules in a fibril may impart time scale differences between loading rates.

The results of our study represent a worst-case scenario for the time course of fatigue damage accumulation in vivo, because the RTTs were nonviable and thus not capable of biological response. Nevertheless, it is clear that repetitive loading causes significant amounts of collagen in RTT to become denatured, even within the range of operational strains experienced by tendons in vivo (*3*). The biological healing process involves both the degradation of damaged tissue via matrix metalloproteinases (MMPs) and the deposition of newly synthesized matrix. Mechanical overload in the presence of MMP activity would further increase the amount of denatured collagen in the tissue. The misregulation of MMP activity and inflammatory factors following damage is also a characteristic of tendon injury (*23*). Thus, the timing and severity of mechanical overloading in concert with in vivo proteolytic activity may potentiate or exacerbate injury by pushing collagen damage beyond the threshold for healthy repair. While tension loading in vitro causes collagen damage, previous studies have demonstrated that a low level of tension is necessary to maintain tendon homeostasis and may impart proteolytic stability to collagen molecules (*24*, *25*). Therefore, it seems likely that homeostatic levels of tendon loading protect the tissue from global enzymatic degradation while promoting controlled tissue turnover via small amounts of loading-induced collagen denaturation.

In most cases, it is evident that a healthy biological response to loading modifies the course of damage accumulation and prevents the development of connective tissue injuries due to normal physical activity. Studies directly investigating cellular collagen production in tendons have revealed increased collagen production and incorporation within hours or days of exercise or direct mechanical loading (*26*, *27*) and have demonstrated circadian regulation of collagen synthesis, cellular export, and degradation as a possible mechanism for maintaining tissue homeostasis (*28*). The exact process by which tendon damage is identified and new collagen is incorporated into noninjured loaded tendons or tendons healing after injury is unclear, but we know that the body has solved this engineering design problem. Research on cell-matrix interactions provides evidence that direct cellular detection of denatured collagen may play a role in initiating the biological healing response. When macrophage-like cells are cultured on mechanically overloaded collagen fibrils exhibiting kinked disruptions that correlate with locations of collagen denaturation, the cells exhibit altered morphology and promote collagen proteolysis (*29*). However, the mechanisms by which this matrix damage is detected are unknown. Human melanoma cells have been demonstrated to recognize fibrillar and denatured collagens by separate integrin subunits via the exposure of Arg-Gly-Asp cryptic sites (*30*), and macrophage scavenger receptors can specifically recognize denatured collagens via their collagenous domain (*31*). Therefore, it is likely that mechanical damage to the collagen molecule in tendon modulates cellular interactions and downstream signaling,

Downloaded from https://www.science.org on October 04, 2021

affecting innate biological mechanisms to repair this damage. The results of the present study are critical for understanding how molecular-level damage accumulates during tendon fatigue. With this foundation, future investigations using in vivo loading and ex vivo organ culture can parse the relative effects of loading-induced damage and cellular remodeling.

Creep deformation and fatigue failure under cyclic subfailure loading are universal material phenomena; however, the damage and failure mechanisms vary widely between material classes. In many engineering materials, discussion of fatigue failure is focused on crack initiation and growth, because these macroscopically observable processes are highly correlated with the final failure of the material. Thus, crack length can be useful for monitoring and to establish service criteria for components subjected to dynamic and oscillatory loads. While some biological materials such as bone may experience fatigue failure in a crack-dominant manner, it is of primary interest to monitor, arrest, and repair damage in soft biological materials before macroscopic tissue separation. Polymer and metal systems can undergo significant plastic deformation before fatigue crack initiation via substructural rearrangement at the micro- to nanoscale (e.g., grain alignment and amorphous phase polymer chain movement). Similarly, fiber-level collagen realignment in the direction of loading is correlated with permanent elongation following preconditioning of ligaments. Most recently, permanent deformation in RTT has been correlated with unrecovered collagen fiber sliding (*32*). However, it remains unclear whether such sliding is truly a mechanism of damage or rather a symptom of more fundamental changes in the collagen structure. Our results, which revealed significant molecular-level collagen damage in this same range of strain, suggest that permanent deformations at higher scales of the collagen hierarchy may be the result of molecular-level disruption. Recent evidence supporting this hypothesis demonstrated that fibril kinking, a ubiquitous indicator of fibril-level collagen damage in positional tendons (*5*), is likely due to unfolding of the collagen triple helix (*33*). The next frontier of understanding damage and repair of dense collagenous tissues will inevitably be to investigate the specific mechanisms by which resident cells sense and respond to collagen molecular damage and to develop methods using triple-helical hybridization to promote and monitor tissue healing.

MATERIALS AND METHODS

Experimental design

This study was designed to examine the hypothesis that molecular-level collagen damage is fundamental to the initiation and progression of fatigue damage in tendon and to identify potential mechanisms of rate-dependent collagen damage and fatigue mechanics. RTT fascicles, from 6-month-old, male Sprague-Dawley rats, were loaded in creep-fatigue across the range from unloaded to failure and stained with F-CHP to detect and quantify denatured collagen. The sample size for CHP quantification was determined on the basis of a power analysis using mean and SD of CHP-binding data from our previous study (*9*). From the power analysis, it was determined that $n = 6$ samples were required to detect an effect size of 0.7, assuming a two-tailed α of 0.05 and a power of 0.8; therefore, 6 samples were collected at each loading condition for F-CHP staining and analysis (72 total samples), and 12 unloaded samples served as negative control. The sample size for fatigue failure tests ($n = 10$ for each strain rate) was not prespecified on the basis of statistical methods, but on prior experience with the sample-to-sample and animal-to-animal variability in tendon stress-strain behavior. Samples were excluded when failure occurred immediately at the interface between the clamp and the sample; in these cases, a new sample was loaded under the same condition. Two samples were excluded from F-CHP quantification due to experimental errors during F-CHP staining. Individual rat tails were randomly selected for strain rate and loading level groups. Finite element and MD computational simulation were used to investigate possible mechanisms of molecular-level collagen damage with repeated loading and mechanisms of strain rate–dependent fatigue mechanics at the fascicle and molecular levels.

Sample preparation and CSA measurement

RTT fascicles were sourced from fresh-frozen, 6-month-old, male Sprague-Dawley rat tails (individual rat tails were purchased from BioIVT, Westbury, NY, USA). Tails were stored at −20°C until use. Individual fascicles were dissected from thawed tails by gripping the distal end of the tail with a hemostat while holding the proximal portion of the tail by hand. The hemostat was twisted around the axis of the tail until the skin separated, and the distal end pulled away to reveal the tendon fascicles. Fascicles were cut away and immediately placed in 1× phosphate-buffered saline (PBS) (pH 7.4) to maintain hydration and osmotically equilibrate.

A custom optical CSA measurement system was used to measure the fascicle CSA accurately for stress calculations (fig. S7). Samples were mounted vertically in the material testing clamps, which were attached to an adjustable z-height stage and rotary motor. Constant humidified air was dispensed onto the sample using an ultrasonic humidifier, and 1× PBS was applied to the clamp interface to maintain sample hydration during measurement. To ensure accurate measurement and reconstruction of the sample geometry, the z height of the top clamp was adjusted just until slack was removed from the sample, indicated by the sample remaining still in the light air movement from the humidifier. Sample width and reference location were measured through a 180° rotational sweep to reconstruct the sample cross section. Samples were rotated using a continuous rotation stage (CR7-Z1, Thorlabs) at a speed of $1° \, s^{-1}$, acquiring measurements every 1 s using an optical micrometer (LS-9006M, Keyence Corporation). Micrometer measurements were acquired at 16 kHz and averaged every 2048 samples using the integrated controller and firmware. Stage rotation and micrometer measurement acquisition were controlled using LabVIEW (National Instruments). The sample profile was then reconstructed using the algorithm of Langelier *et al.* (*34*), implemented in MATLAB (R2016b, MathWorks), and the area enclosed was calculated using the polyarea function. For each sample, cross-sectional measurements were performed at five locations along the length of the sample, at 5-mm increments, and the average area from the five locations was used for nominal stress calculation. Following CSA measurement, the sample clamps were mounted at a fixed distance to prevent overloading of the sample during transfer between the CSA measurement and material test systems.

Fatigue testing

Following CSA measurement, samples were transferred to the material test system (ElectroForce 3300 Series II, TA Instruments). Sample hydration during testing was maintained by immersion in room temperature 1× PBS at pH 7.4. To establish stress levels for fatigue testing, RTT fascicles were monotonically loaded to failure at $1\% \, s^{-1}$ ($n = 8$ samples). The maximum force was normalized to

Downloaded from https://www.science.org on October 04, 2021

the initial CSA to determine the mean UTS (46.23 ± 7.73 MPa; mean ± SD). Samples were preconditioned before fatigue loading to establish consistent material response. A 0.03 N preload was established, and samples were cycled between 0.1 N and 4.6 MPa (10% of the failure strength at 1% s^{-1} monotonic tension loading) for 11 cycles at 0.06% s^{-1} using a triangle waveform. In pilot testing, the 0.06% s^{-1} strain rate was found to produce approximately 1-Hz loading at the defined preconditioning stress level. Following preconditioning, samples were unloaded (remaining in testing clamps) and allowed to recover for 5 min. A 0.03 N preload was reestablished, and the zero-strain length was calculated. Samples were then loaded between 0.2 N and 18.5 MPa (40% of the failure strength at 1% s^{-1} monotonic tension loading) at 0.4, 4, or 40% s^{-1} using a triangle waveform until failure (n = 10 per loading rate). The 4% s^{-1} strain rate was found to produce approximately 1-Hz loading at 50% of the cycles to failure during pilot testing. The additional strain rates were then chosen to be one decade above and below this effective 1-Hz loading. Samples loaded to fatigue failure were used to establish the average creep behavior of RTT fascicles and to generate the failure group for CHP detection of denatured collagen (n = 6 per loading rate randomly selected from each group of 10 samples for CHP staining).

To understand the role of molecular-level collagen damage across the spectrum from unloaded to fatigue failure, additional fascicles were tested to incremental levels of fatigue. Because of the large range in number of cycles to failure, the number of loading cycles was not an appropriate parameter to establish incremental levels of fatigue loading. However, the creep strain was much more consistent, as a percentage of number of cycles to failure. Therefore, the mean creep strain (strain at the peak of the loading cycle) of fatigue failure samples, at 20, 50, and 80% of cycles to failure, was used to define incremental fatigue levels (Fig. 1A). Samples were preconditioned as described, and then loaded in creep-fatigue between 0.2 N and 18.5 MPa at 0.4, 4, or 40% s^{-1} until reaching one of the defined incremental strain levels ($n \geq 5$ at each strain level and loading rate; one sample from the 4% s^{-1} 80% incremental group and one sample from the 4% s^{-1} failure group were excluded from analysis due to experimental error during F-CHP staining resulting in five samples for each of those two groups), at which point the sample was immediately unloaded. Following testing, samples were removed from the test clamps, and the clamped ends of the sample were cut away to isolate the loaded region for collagen damage quantification. Unloaded samples served as control. To ensure that there was no concern of protease activity during fatigue testing, additional samples were stored in 1× PBS supplemented with protease inhibitors (2 mM EDTA and 5 mM benzamidine HCl) or subjected to approximately 1 hour of additional room temperature storage in unsupplemented 1× PBS before testing to fatigue failure. There was not a significant difference in the number of cycles to failure (fig. S8) for either of these groups when compared to control samples tested in unsupplemented 1× PBS, indicating that protease activity was not of concern for the duration of fatigue loading in this study. All samples were stored at −70°C in 1× PBS until CHP staining.

CHP staining and quantification

To detect and quantify denatured collagen, control and fatigue-loaded samples were stained using F-CHP (Fig. 1B). The wet weight of the samples was measured to normalize fluorescence data by sample mass. First, liquid was removed from the surface of samples by blotting on a laboratory wipe, and then samples were immersed into a vial of 1× PBS of known mass on an analytical laboratory balance (ME304, Mettler Toledo). This measurement was repeated three times for each sample, and the mean value was used for normalization. Samples were then stained overnight in 15 μM F-CHP (5-FAM conjugate CHP, 3Helix Inc.). F-CHP stock solution (150 μM) was heated at 80°C for 10 min to thermally dissociate trimeric CHP to a monomeric state and quenched by immersion in 4°C water for 15 s. Each fascicle was placed in a vial containing 450 ml of 1× PBS, and 50 ml of monomeric F-CHP stock was added, resulting in a final F-CHP concentration of 15 μM. Fascicles were incubated overnight at 4°C, and then unbound F-CHP was removed by washing three times in 1 ml of 1× PBS for 30 min at room temperature.

To quantify F-CHP fluorescence, stained samples were digested in 500 μl of proteinase K (1 mg/ml) in water for 3 hours at 60°C. Following digestion, 200 μl from each sample was pipetted into a 96-well plate, and samples were measured in duplicate at 485- and 525-nm excitation and emission, respectively (SpectraMax M4, Molecular Devices). Fluorescence values were normalized to the sample wet weight. The amount of denatured collagen present was calculated from normalized fluorescence using a standard curve for RTT fascicles relating normalized CHP fluorescence to denatured collagen as measured by the trypsin digestion assay for denatured collagen (*15*).

Biphasic finite-element simulation

Finite-element simulations were conducted using a representative, idealized fascicle geometry, representing a cross section at the middle of the test sample (Fig. 1C). A quarter cylinder of 156-μm radius and 2:1 length-to-radius ratio was meshed using 16 six-noded pentagonal and 240 eight-noded hexagonal elements. The mesh density was determined by a convergence test that showed less than 0.1% difference in axial displacement, at the peaks of the cyclic waveform, upon further mesh refinement. The quarter cylinder model was loaded in uniaxial tension with symmetry boundary conditions. This radius was calculated from the circular radius for the average CSA of tested RTT fascicles. The outer surface of the cylinder was set to be free-draining, and all other surfaces were modeled as impermeable. Creep load was applied to the top surface of the cylinder via a rigid body contact interface. Displacements at the top and bottom surfaces were only constrained or prescribed in the axial direction. Simulation was performed using FEBio software (*35*). The tendon material was represented using a biphasic formulation with a large Poisson's ratio elastic solid material with mobile fluid phase (*36*). Solid material parameters were determined by optimizing the elastic material response to quasistatic material test experimental data, and permeability was set within the range of intrinsic permeability measured for tendon (*37*). The Poisson's penalty parameter, which affects the solid material time-dependent response in biphasic simulations, was determined by optimizing the model response to five cycles of experimental creep-fatigue loading data. Material parameters used for all simulations are listed in table S1. Cyclic load was applied to match experimental levels of 0.2 N to 18.5 MPa.

Simulation of collagen model peptides

A representative homotrimeric collagen peptide composed of 20 (Gly-Pro-Hyp) triplets was generated by the Triple Helical collagen Building Script (*38*). The atomistic simulations of the collagen peptide were performed via LAMMPS (large-scale atomic/molecular massively parallel simulator) (*39*) using the CHARMM force field in simulation boxes of 25 nm by 5 nm by 5 nm. Then, the box was

Downloaded from https://www.science.org on October 04, 2021

solvated in explicit water molecules and neutralized with 0.5 M NaCl (Fig. 1D). The long-range Coulombic interaction was calculated by the particle-particle particle-mesh method (*40*) with periodic boundary conditions in all three directions. After energy minimization, we used the Berendsen barostat and thermostat (NPT ensemble) to relax the simulation box at 1 atm and 310 K before relaxing the system in the NVT ensemble at 310 K for 0.5 ns with a 1-fs time step. A 2-fs time step with a constraint for the hydrogen bond tends to be numerically unstable when the SMD is applied. During the relaxation, the ends of the collagen peptide were anchored with a small force of 5 kcal/molÅ (350 pN) to prevent peptide bending.

We designed the cyclic loading based on the maximum and minimum forces using SMD. The minimum force was required to make the collagen molecule straightened and is consistent with the experimental condition, as in Fig. 1A. We considered two different boundary conditions, as in Fig. 1D. One condition was normal tensile loading (i.e., tension-dominant) with the edges of three chains bound to the SMD spring during the cyclic loading. The other condition was shear loading (i.e., shear-dominant) with only a single chain under the cyclic loading. In both boundary conditions, a pulling spring constant was set to 10 kcal/molÅ^2.

The cyclic SMD was applied to deform the molecule between 350 pN (5 kcal/molÅ) and 2085 pN (30 kcal/molÅ) with constant loading and unloading speeds of 3, 5, 10, or 20 m/s. Because of the computational limitations imposed by the maximum time step that can be taken in MD simulations, it was not feasible to match the experimental and simulated loading rates. These rates were selected to span an order of magnitude range and inform our understanding of the rate dependence of triple-helix unfolding. The strains were recorded on the basis of the position of SMD spring. SASA with a probe radius of 1.4 Å, a measure of molecular unfolding, and the number of hydrogen bonds with the cutoff distance and angle of 4.0 Å and 35°, respectively, were computed from the loading simulations.

Statistical analysis

Experimental data were analyzed using mixed-effects linear regression, accounting for the grouping of samples within animals. Log transformation was used for models demonstrating logarithmic scaling of the independent or dependent variables, as demonstrated by improved goodness of fit (R^2) compared to the untransformed regression. For models containing multiple independent variables (e.g., loading rate and incremental fatigue level for denatured collagen), an interaction term was included in the regression model. Significance of the model coefficients was established at the $\alpha = 0.05$ level. All regression models were performed in Stata (IC 15.1, StataCorp) using the xtreg command for random-effects linear regression and the panel variable option to account for multiple samples taken from each rat tail; all other command options were unchanged from default.

SUPPLEMENTARY MATERIALS

Supplementary material for this article is available at http://advances.sciencemag.org/cgi/content/full/6/35/eaba2795/DC1

View/request a protocol for this paper from *Bio-protocol*.

REFERENCES AND NOTES

1. W. B. Leadbetter, Cell-matrix response in tendon injury. *Clin. Sports Med.* **11**, 533–578 (1992).
2. H. Schechtman, D. L. Bader, In vitro fatigue of human tendons. *J. Biomech.* **30**, 829–835 (1997).
3. R. F. Ker, X. T. Wang, A. V. Pike, Fatigue quality of mammalian tendons. *J. Exp. Biol.* **203**, 1317–1327 (2000).
4. D. T. Fung, V. M. Wang, N. Andarawis-Puri, J. Basta-Pljakic, Y. Li, D. M. Laudier, H. B. Sun, K. J. Jepsen, M. B. Schaffler, E. L. Flatow, Early response to tendon fatigue damage accumulation in a novel in vivo model. *J. Biomech.* **43**, 274–279 (2010).
5. T. W. Herod, N. C. Chambers, S. P. Veres, Collagen fibrils in functionally distinct tendons have differing structural responses to tendon rupture and fatigue loading. *Acta Biomater.* **42**, 296–307 (2016).
6. S. E. Szczesny, C. Aeppli, A. David, R. L. Mauck, Fatigue loading of tendon results in collagen kinking and denaturation but does not change local tissue mechanics. *J. Biomech.* **71**, 251–256 (2018).
7. B. R. Freedman, A. Zuskov, J. J. Sarver, M. R. Buckley, L. J. Soslowsky, Evaluating changes in tendon crimp with fatigue loading as an ex vivo structural assessment of tendon damage. *J. Orthop. Res.* **33**, 904–910 (2015).
8. T. A. Wren, D. P. Lindsey, G. S. Beaupré, D. R. Carter, Effects of creep and cyclic loading on the mechanical properties and failure of human Achilles tendons. *Ann. Biomed. Eng.* **31**, 710–717 (2003).
9. J. L. Zitnay, Y. Li, Z. Qin, B. H. San, B. Depalle, S. P. Reese, M. J. Buehler, S. M. Yu, J. A. Weiss, Molecular level detection and localization of mechanical damage in collagen enabled by collagen hybridizing peptides. *Nat. Commun.* **8**, 14913 (2017).
10. Y. Li, D. Ho, H. Meng, T. R. Chan, B. An, H. Yu, B. Brodsky, A. S. Jun, S. Michael Yu, Direct detection of collagenous proteins by fluorescently labeled collagen mimetic peptides. *Bioconjug. Chem.* **24**, 9–16 (2013).
11. S. P. Veres, J. M. Harrison, J. M. Lee, Mechanically overloading collagen fibrils uncoils collagen molecules, placing them in a stable, denatured state. *Matrix Biol.* **33**, 54–59 (2014).
12. T. L. Willett, R. S. Labow, N. C. Avery, J. M. Lee, Increased proteolysis of collagen in an in vitro tensile overload tendon model. *Ann. Biomed. Eng.* **35**, 1961–1972 (2007).
13. R. J. Minns, F. S. Steven, Local denaturation of collagen fibres during the mechanical rupture of collagenous fibrous tissue. *Ann. Rheum. Dis.* **39**, 164–167 (1980).
14. J. H. Shepherd, H. R. Screen, Fatigue loading of tendon. *Int. J. Exp. Pathol.* **94**, 260–270 (2013).
15. A. H. Lin, J. L. Zitnay, Y. Li, S. M. Yu, J. A. Weiss, Microplate assay for denatured collagen using collagen hybridizing peptides. *J. Orthop. Res.* **37**, 431–438 (2019).
16. N. C. Heglund, C. R. Taylor, T. A. McMahon, Scaling stride frequency and gait to animal size: Mice to horses. *Science* **186**, 1112–1113 (1974).
17. G. A. Cavagna, P. Franzetti, N. C. Heglund, P. Willems, The determinants of the step frequency in running, trotting and hopping in man and other vertebrates. *J. Physiol.* **399**, 81–92 (1988).
18. R. C. Haut, Age-dependent influence of strain rate on the tensile failure of rat-tail tendon. *J. Biomech. Eng.* **105**, 296–299 (1983).
19. B. N. Safa, K. D. Meadows, S. E. Szczesny, D. M. Elliott, Exposure to buffer solution alters tendon hydration and mechanics. *J. Biomech.* **61**, 18–25 (2017).
20. B. K. Connizzo, A. J. Grodzinsky, Tendon exhibits complex poroelastic behavior at the nanoscale as revealed by high-frequency AFM-based rheology. *J. Biomech.* **54**, 11–18 (2017).
21. S. P. Reese, J. A. Weiss, Tendon fascicles exhibit a linear correlation between Poisson's ratio and force during uniaxial stress relaxation. *J. Biomech. Eng.* **135**, 34501 (2013).
22. G. Jung, Z. Qin, M. J. Buehler, Mechanical properties and failure of biopolymers: Atomistic reactions to macroscale response. *Top. Curr. Chem.* **369**, 317–343 (2015).
23. P. Sharma, N. Maffulli, Tendon injury and tendinopathy: Healing and repair. *J. Bone Joint Surg. Am.* **87**, 187–202 (2005).
24. M. Lavagnino, S. P. Arnoczky, T. Tian, Z. Vaupel, Effect of amplitude and frequency of cyclic tensile strain on the inhibition of MMP-1 mRNA expression in tendon cells: An in vitro study. *Connect. Tissue Res.* **44**, 181–187 (2003).
25. S.-W. Chang, B. P. Flynn, J. W. Ruberti, M. J. Buehler, Molecular mechanism of force induced stabilization of collagen against enzymatic breakdown. *Biomaterials* **33**, 3852–3859 (2012).
26. H. Langberg, D. Skovgaard, L. J. Petersen, J. Bulow, M. Kjaer, Type I collagen synthesis and degradation in peritendinous tissue after exercise determined by microdialysis in humans. *J. Physiol.* **521**, 299–306 (1999).
27. H. R. C. Screen, J. C. Shelton, D. L. Bader, D. A. Lee, Cyclic tensile strain upregulates collagen synthesis in isolated tendon fascicles. *Biochem. Biophys. Res. Commun.* **336**, 424–429 (2005).
28. J. Chang, R. Garva, A. Pickard, C.-Y. C. Yeung, V. Mallikarjun, J. Swift, D. F. Holmes, B. Calverley, Y. Lu, A. Adamson, H. Raymond-Hayling, O. Jensen, T. Shearer, Q. J. Meng, K. E. Kadler, Circadian control of the secretory pathway maintains collagen homeostasis. *Nat. Cell Biol.* **22**, 74–86 (2020).
29. S. P. Veres, E. P. Brennan-Pierce, J. M. Lee, Macrophage-like u937 cells recognize collagen fibrils with strain-induced discrete plasticity damage. *J. Biomed. Mater. Res. A* **103**, 397–408 (2015).

Downloaded from https://www.science.org on October 04, 2021

30. G. E. Davis, Affinity of integrins for damaged extracellular matrix: $\alpha_v\beta_3$ binds to denatured collagen type I through RGD sites. *Biochem. Biophys. Res. Commun.* **182**, 1025–1031 (1992).
31. B. B. Gowen, T. K. Borg, A. Ghaffar, E. P. Mayer, The collagenous domain of class a scavenger receptors is involved in macrophage adhesion to collagens. *J. Leukoc. Biol.* **69**, 575–582 (2001).
32. A. H. Lee, S. E. Szczesny, M. H. Santare, D. M. Elliott, Investigating mechanisms of tendon damage by measuring multi-scale recovery following tensile loading. *Acta Biomater.* **57**, 363–372 (2017).
33. J. M. Lee, S. P. Veres, Advanced glycation end-product cross-linking inhibits biomechanical plasticity and characteristic failure morphology of native tendon. *J. Appl. Physiol.* **126**, 832–841 (2019).
34. E. Langelier, D. Dupuis, M. Guillot, F. Goulet, D. Rancourt, Cross-sectional profiles and volume reconstructions of soft tissues using laser beam measurements. *J. Biomech. Eng.* **126**, 796–802 (2004).
35. S. A. Maas, B. J. Ellis, G. A. Ateshian, J. A. Weiss, FEBio: Finite elements for biomechanics. *J. Biomech. Eng.* **134**, 011005 (2012).
36. A. M. Swedberg, S. P. Reese, S. A. Maas, B. J. Ellis, J. A. Weiss, Continuum description of the Poisson's ratio of ligament and tendon under finite deformation. *J. Biomech.* **47**, 3201–3209 (2014).
37. B. N. Safa, E. T. Bloom, A. H. Lee, M. H. Santare, D. M. Elliott, Evaluation of transverse poroelastic mechanics of tendon using osmotic loading and biphasic mixture finite element modeling. *J. Biomech.* **109**, 109892 (2020).
38. J. K. Rainey, M. C. Goh, An interactive triple-helical collagen builder. *Bioinformatics* **20**, 2458–2459 (2004).
39. S. Plimpton, Fast parallel algorithms for short-range molecular dynamics. *J. Comput. Phys.* **117**, 1–19 (1995).
40. E. L. Pollock, J. Glosli, Comments on P^3M, FMM, and the Ewald method for large periodic coulombic systems. *Comput. Phys. Commun.* **95**, 93–110 (1996).

Acknowledgments: We thank G. Stoddard of the University of Utah Biostatistics and Study Design core for assistance with the statistical method development. **Funding:** This work was supported by the NIH (F31EB023086 to J.L.Z.; R01AR071358 to J.A.W. and S.M.Y.; U01EB014976 to G.S.J., Z.Q., and M.J.B.) and the Office of Naval Research (N00014-16-1-233 to G.S.J., Z.Q., and M.J.B.). **Author contributions:** J.L.Z. and J.A.W. designed the tendon fatigue experiments and finite-element simulations. J.L.Z. performed fatigue experiments and finite-element simulations. A.H.L. assisted with CHP quantification and analysis. G.S.J., Z.Q., and M.J.B. designed the MD simulations. G.S.J. performed MD simulations and analysis. A.H.L., Y.L., and S.M.Y. contributed to the study design and analysis. J.L.Z., G.S.J., and J.A.W. wrote the manuscript. A.H.L., S.M.Y., and M.J.B. provided manuscript feedback and edits. **Competing interests:** S.M.Y. and Y.L. are co-founders of 3Helix Inc. The other authors declare that they have no competing interests. **Data and materials availability:** All data needed to evaluate the conclusions in the paper are present in the paper and/or the Supplementary Materials. Additional data related to this paper may be requested from the authors. The LAMMPS open-source code is publicly available at http://lammps.sandia.gov.

Submitted 22 January 2020
Accepted 14 July 2020
Published 28 August 2020
10.1126/sciadv.aba2795

Citation: J. L. Zitnay, G. S. Jung, A. H. Lin, Z. Qin, Y. Li, S. M. Yu, M. J. Buehler, J. A. Weiss, Accumulation of collagen molecular unfolding is the mechanism of cyclic fatigue damage and failure in collagenous tissues. *Sci. Adv.* **6**, eaba2795 (2020).

Downloaded from https://www.science.org on October 04, 2021

ScienceAdvances

Accumulation of collagen molecular unfolding is the mechanism of cyclic fatigue damage and failure in collagenous tissues

Jared L. ZitnayGang Seob JungAllen H. LinZhao QinYang LiS. Michael YuMarkus J. BuehlerJeffrey A. Weiss

Sci. Adv., 6 (35), eaba2795.

View the article online
https://www.science.org/doi/10.1126/sciadv.aba2795
Permissions
https://www.science.org/help/reprints-and-permissions

Downloaded from https://www.science.org on October 04, 2021

Use of think article is subject to the Terms of service

Science Advances (ISSN 2375-2548) is published by the American Association for the Advancement of Science. 1200 New York Avenue NW, Washington, DC 20005. The title *Science Advances* is a registered trademark of AAAS.
Copyright © 2020 The Authors, some rights reserved; exclusive licensee American Association for the Advancement of Science. No claim to original U.S. Government Works. Distributed under a Creative Commons Attribution NonCommercial License 4.0 (CC BY-NC).